npj | Clean Water

www.nature.com/npjcleanwater

ARTICLE OPEN

Check for updates

Nanosilica modified with polyaspartic acid as an industrial circulating water scale inhibitor

Yamin Cheng[1,2,3,4], Xinyu Guo[1,2,3,4], Xiaowei Zhao[1,3], Yufeng Wu[1,3], Zhongyan Cao[1,3], Yonghong Cai[1]✉ and Ying Xu[1,2,3]✉

Given the special performance of nanosilica with its small size, large specific surface area and high surface activity, nanosilica containing reactive amino group (denoted as SiO_2–NH_2) and polysuccinimide were allowed to take part in polymerization reaction to afford SiO_2–NH_2 modified polyaspartic acid (denoted as SiO_2–NH_2/PASP), a potential polymer scale inhibitor with good water solubility for industrial circulating water. The scale inhibition performance of the as-prepared SiO_2–NH_2/PASP was evaluated by static scale inhibition test; and its scale inhibition mechanism was explored by means of scanning electron microscopy, X-ray diffraction, and X-ray photoelectron spectroscopy. Results indicated that SiO_2–NH_2/PASP exhibits excellent scale inhibition performance against $CaSO_4$ and $CaCO_3$ at very low concentrations (optimum scale inhibition rate of 100% and 68%, respectively), and the presence of 5 mg/L of SiO_2–NH_2/PASP greatly increases the inhibition efficiency of $CaSO_4$ and $CaCO_3$ scale by 21% and 53%, obviously higher than that of pure PASP.

npj Clean Water (2021)4:46 ; https://doi.org/10.1038/s41545-021-00137-y

INTRODUCTION

The pipeline inner walls of circulating cooling water system often face the challenge of inorganic scale deposition upon exposure to a large amount of poorly soluble inorganic salts, which could cause huge economic losses and operational problems in facilities such as reverse osmosis desalination system, multi-stage flash desalination system, and multi-effect distillation system[1–3].

Therefore, it is imperative to introduce a scale inhibitor to get rid of the scale formation on the inner walls of the pipelines of industrial circulating water. Some plant extracts and phosphorous compounds are of particular significance for inhibiting scale formation[4,5]. For example, Gambier extract as a green inhibitor can efficiently inhibit the scale formation of calcium carbonate; and the natural extract of tobacco rob can function as a scale- and corrosion-inhibitor in artificial seawater[6,7]. The reason lies in that the plant extracts contain a large amount of amino and carboxyl functionalities which have the strong complexing ability with Ca^{2+}. However, the huge amount of plant extracts could cause potentially deteriorating the ecological environment[8]; and phosphorous compounds might lead to serious environmental risks of water eutrophication[9,10]. Therefore, the exploitation of environmentally friendly scale inhibitors for water treatment is of vital importance.

Polyaspartic acid (denoted as PASP) as an environmentally friendly additive is nontoxic, biodegradable, and free of phosphorus[10–12]. However, its scale inhibition performance is poor, which limits its application in the industry. Since the scale inhibition performance of polymer scale inhibitors is highly dependent on their carboxyl, hydroxyl, and acylamido groups with strong ionic chelating ability[13–15], we introduce these functional groups into the PASP molecule through the copolymerization of L-aspartic acid or the ring-opening modification of polysuccinimide (denoted as PSI) to obtain functionalized PASP with improved scale inhibition performance. The copolymerization modification mainly involves the reaction of aspartic acid with other monomers, which, in combination with the introduction of other functional groups into the molecular chain of aspartic acid, could contribute to improving the scale inhibition performance to some extent. For example, Dong et al.[16] reported that curcumin, a fluorescent monomer, can be introduced into the PASP molecular chain in the presence of L-aspartic acid and citric acid; and the as-synthesized scale inhibitor exhibits superior fluorescent-tagged properties and excellent scale inhibition performance. However, L-aspartic acid is expensive and faces challenges with industrial production. Fortunately, highly active linear PSI can be easily cyclized by amino to form PASP with side chains[17], which provides a feasible pathway to yielding functionalized PASP. Chen et al.[18] reported an interesting exploration in this respect: they synthesized a scale inhibitor with PSI and histidine as the starting materials. Thanks to the introduction of an amino group and carboxyl group to inhibit the reaction crystallization of Ca-scale crystals, the as-synthesized PASP-based scale inhibitor has a promising anti-scaling ability. Similarly, Xu et al.[19] introduced hydroxyl into the side chain of PASP with PSI and 2-amino-2-methyl-1-propanol (AMP) as raw materials. The as-obtained PASP/AMP exhibits improved scale- and corrosion-inhibition performances, and its biodegradation rate is acceptable in terms of the Convention for the Protection of the Marine Environment of the Northeast Atlantic[20]. These researches demonstrate that introducing strong chelating groups into PASP molecular chain through ring-opening reaction is favorable for improving the scale inhibition performance; and the ring-opening reaction, with desired environmental acceptance, could be of special significance for the development of polymer–matrix scale inhibitor.

Viewing the abovementioned perspectives, here we attempt to introduce amino-functionalized silicon dioxide into the ring-opening reaction of PSI, hoping to obtain a modified PASP scale inhibitor with improved scale inhibition performance. We pay special attention to amino-functionalized nano-silica (nano-SiO_2) with small size, large specific surface area, high surface activity,

[1]College of Chemistry and Chemical Engineering, Henan University, Kaifeng 475004, China. [2]Engineering Research Center for Water Environment and Health of Henan, Zhengzhou University of Industrial Technology, Zhengzhou 451150, China. [3]Engineering Research Center for Industrial Recirculating Water Treatment, Henan University, Kaifeng 475004, China. [4]These authors contributed equally: Yamin Cheng, Xinyu Guo. ✉email: caiyonghong@henu.edu.cn; hdccxu@126.com

and multiple reaction sites, because it has been found to be intriguing in the petroleum industry, electronics industry and coating industry and so on[21–24]. The surface-capped nano-SiO_2 has little steric hindrance and contains many reaction sites, and it can react with PSI to generate SiO_2–NH_2/PASP containing organic functional groups that can chelate with calcium ions, thereby effectively preventing scaling. This article deals with the preparation of SiO_2–NH_2/PASP, a potential green scale inhibitor applicable to the industrial circulating water system; and it also reports its scale inhibition performance and mechanism.

RESULTS AND DISCUSSION

Synthesis and structural characterization of SiO_2–NH_2/PASP

The TEM image of SiO_2–NH_2 nanoparticles is shown in Fig. S1. It can be seen that SiO_2–NH_2 nanoparticles appear as aggregates and have a size of about 10–20 nm. The synthetic route of SiO_2–NH_2/PASP scale inhibitor is shown in Fig. 1. There is a large amount of amino group on the surface of SiO_2–NH_2; and PASP is connected to the surface of nano-silica by CO–NH covalent bond. As a result, the as-synthesized SiO_2–NH_2/PASP product contains a large amount of amide group and carboxyl group that can inhibit the formation of scale.

The FTIR spectra of SiO_2–NH_2/PASP and PASP are shown in Fig. 2a. The stretching vibration absorbance peaks of N–H, C=O, and C–N in the amide bond appear at 3417 cm^{-1}, 1624 cm^{-1}, and 1402 cm^{-1}, respectively; and these FTIR data prove that PSI successfully participates in ring-opening reaction to generate PASP[25]. The asymmetric stretching vibration and stretching vibration peaks of Si–O–Si can be detected at 1053 and 872 cm^{-1}, respectively[26]. This indicates that SiO_2–NH_2 is involved in the polymerization of PSI yielding SiO_2–NH_2/PASP. Figure 2b shows the ^{1}H NMR spectra of SiO_2–NH_2/PASP in D_2O. The signals at 4.5 and 2.8 ppm are assigned to -CH- and -CH_2- of SiO_2–NH_2/PASP, respectively. The FTIR and ^{1}H NMR data give good evidence of the successful synthesis of SiO_2–NH_2/PASP.

The EDS characterization and Si element mapping of SiO_2–NH_2/PASP are shown in Fig. S2. The Si peak is assigned to SiO_2–NH_2 in the as-synthesized SiO_2–NH_2/PASP scale inhibitor (Fig. S2a). The uniform Si element distribution in SiO_2-NH_2/PASP indicates that SiO_2–NH_2 nanoparticles do not agglomerate therein while they participate in the polymerization reaction (Fig. S2b).

To further verify the successful synthesis of SiO_2–NH_2/PASP scale inhibitor, we synthesized PASP under the same conditions for synthesizing SiO_2–NH_2/PASP. The as-obtained PASP was then mixed with SiO_2–NH_2 under 10 min of mechanical stirring. The mixed dispersion of PASP and SiO_2–NH_2 tends to sediment at the bottom of the beaker; and that of the as-synthesized SiO_2–NH_2/PASP is homogeneous, possibly due to the bonding of a large amount of PASP molecular chains on the surface of SiO_2–NH_2. This further proves that the ring-opening reaction of PSI in the presence of SiO_2–NH_2 indeed gives rise to SiO_2–NH_2/PASP.

One milliliter of PASP and SiO_2–NH_2/PASP solutions of 0.0230 and 0.0166 g/mL were taken into two beakers, respectively, acidified to pH ≈2 with 0.1 mol/L HCl solution, then diluted and shaken with 10 mL distilled water, titrated with 0.104 mol/L NaOH standard solution. When 0.108 mL was added to each drop, the primary conductivity value was recorded. The titration curve is shown in Fig. S3. The carboxyl group contents of PASP and SiO_2–NH_2/PASP were calculated to be 15.06% and 15.59%, respectively.

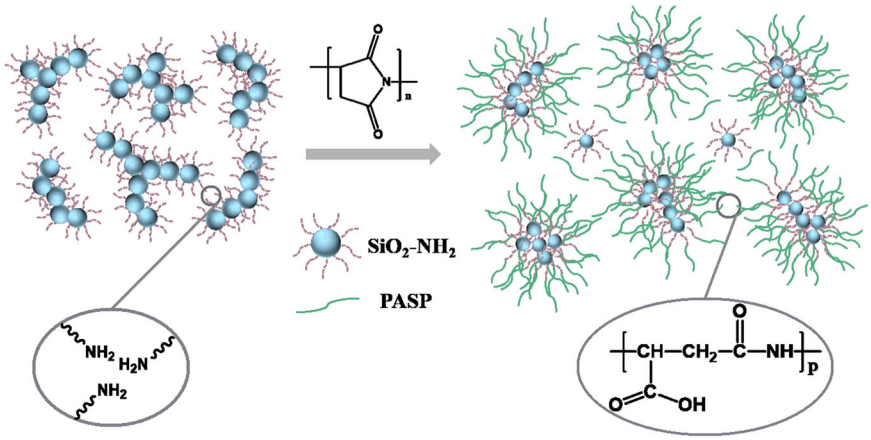

Fig. 1 Synthesis route of SiO_2-NH_2/PASP scale inhibitor. SiO_2-NH_2 nanosilica containing reactive amino group, PASP polyaspartic acid.

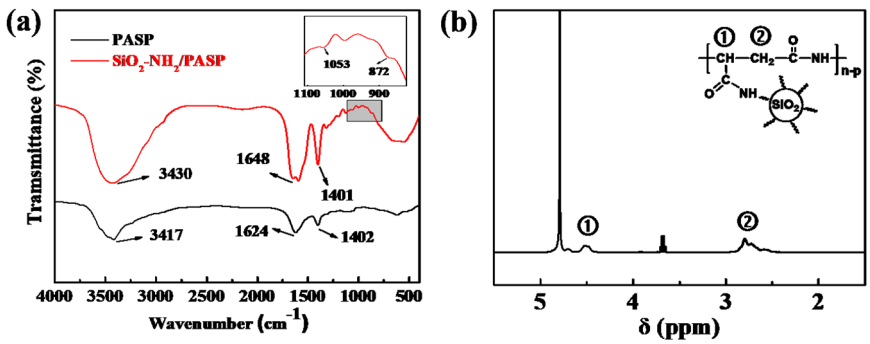

Fig. 2 Structural characterization of polymer. a FTIR spectra of PASP and SiO_2–NH_2/PASP, **b** ^{1}H NMR spectra of SiO_2–NH_2/PASP.

Effect of SiO_2–NH_2/PASP against $CaSO_4$ and $CaCO_3$ scales

Figure 3 shows the variations of scale inhibition efficiency with inhibitor concentration as well as static inhibition test temperature and time. Generally, the as-synthesized SiO_2–NH_2/PASP exhibits better scale inhibition performance than PASP; and its scale inhibition efficiency varies diversely with varying concentration as well as static inhibition test temperature and time. The inhibitory performance of SiO_2–NH_2/PASP with 5 mg/L was 21% higher than that of the unmodified PASP (Fig. 3a). Particularly, the scale inhibition efficiency of SiO_2–NH_2/PASP reaches the maximum of nearly 100% at a concentration of 6 mg/L. We further explore the influence of the dosage of PASP and SiO_2–NH_2/PASP on the inhibition rate of $CaSO_4$, as is shown in Fig. S4. In the absence of a scale inhibitors, a large amount of calcium sulfate precipitate is formed. After the addition of PASP inhibitor, there is a little scale at the bottom of the conical flask; and there is nearly no scale after the introduction of 5 mg/L SiO_2–NH_2/PASP. This indicates that SiO_2–NH_2/PASP can effectively prevent the formation of the $CaSO_4$ scale. The reason might lie in that the carboxylic group of SiO_2–NH_2/PASP can coordinate with calcium ions to adsorb free calcium ions in the solution, and thus reduce the combination of Ca^{2+} and sulfate ions, to prevent the generation of $CaSO_4$ scale[27]. As can be seen from Fig. S3, compared with PASP, the carboxyl group content in the molecular structure of SiO_2–NH_2/PASP is higher, indicating that SiO_2–NH_2/PASP exhibits more excellent scale inhibition performance.

Static inhibition test temperature also plays an important role in the scale inhibition performance. As shown in Fig. 3b, the scale inhibition efficiency of SiO_2–NH_2/PASP decreases rapidly with rising test temperature; and that of SiO_2–NH_2/PASP remains at nearly 100% in the temperature range of 70–75 °C. Besides, SiO_2–NH_2/PASP with the optional concentration of 6 mg/L always exhibits much higher scale inhibition efficiency than PASP in the whole temperature range of static inhibition test; and the scale inhibition efficiency tends to decline at the higher static inhibition test temperature. Yang reported that "the nucleation rate of $CaSO_4$ scale can be influenced by temperature and supersaturation ratio (S)[28,29]. The temperature has little effect on S. When S remains constant, the higher the temperature is, the higher the nucleation rate is, and the easier scaling is[29,30].

$$J = A \cdot exp\left[-\frac{\beta\gamma^3 V_m^2 f(\theta)}{k^3 T^3 (lnS)^2}\right] \quad (1)$$

where A is a frequency factor, β is a geometric (shape) factor of 16 π/3 for the spherical nucleus, and $f(\theta)$ is a correction factor, when heterogeneous nucleation occurs $f(\theta) = 0.01$[31]. V_m is the molar volume of the phase forming, γ is the surface energy (J/m^2). S is the supersaturation ratio, k is the Boltzmann constant, T is the absolute temperature[29]."

Moreover, SiO_2–NH_2/PASP (at the optimal dosage of 6 mg/L) has excellent inhibition performance against the $CaSO_4$ scale over a long test time; and its inhibition efficiency stays nearly at 100% after 25 h of static scale inhibition test (Fig. 3c). It is possible that the chelation stability between PASP and calcium ions becomes worse with the increase of test time, leading to the decrease of scale inhibition efficiency. This demonstrates that SiO_2–NH_2/PASP exhibits excellent scale inhibition performance and could have promising potential for industrial water treatment.

Figure 4 shows the static scale-inhibition performance of SiO_2–NH_2/PASP and PASP against calcium carbonate precipitate. The inhibition efficiency of SiO_2–NH_2/PASP on the $CaCO_3$ scale is significantly higher than that of pure PASP. Particularly, at a concentration of 5 mg/L, the complexation and solubilization effect of SiO_2–NH_2/PASP for $CaCO_3$ is increased by 53% as compared with those of the PASP scale inhibitor (Fig. 4a). This is caused by the chelation of the carboxyl group in the scale inhibitor molecule and calcium ions. The results in combination with Fig. S3 show that SiO_2–NH_2/PASP has more carboxyl group content and is easier to combine with the free calcium ions in the solution compared with PASP, thus inhibiting the formation of calcium carbonate scale. The scale inhibition efficiency initially increases with increasing concentration of SiO_2–NH_2/PASP; and the inhibition efficiency of SiO_2–NH_2/PASP is close to 68% under an inhibitor concentration of 30 mg/L. After that, the inhibition efficiency remains stable with increasing concentration, showing a so-called "threshold effect". This is because, on the one hand,

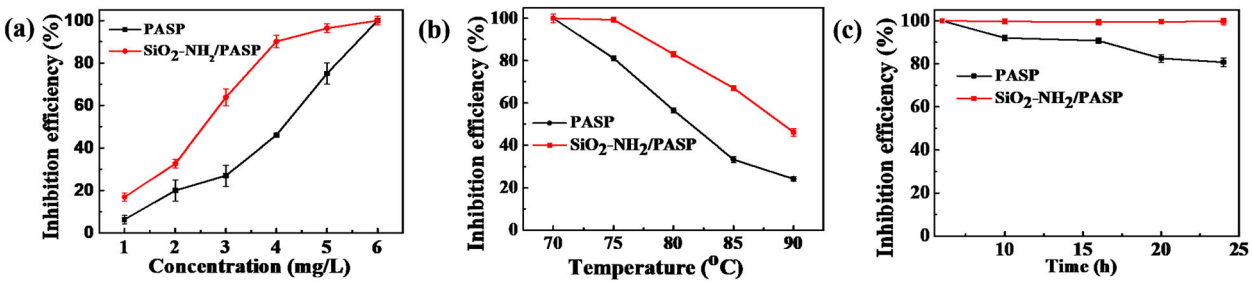

Fig. 3 Inhibition efficiency of PASP and SiO_2–NH_2/PASP against $CaSO_4$ scale. a different inhibitor concentration, **b** different test temperature, **c** different test time. Error bars indicate the standard deviation.

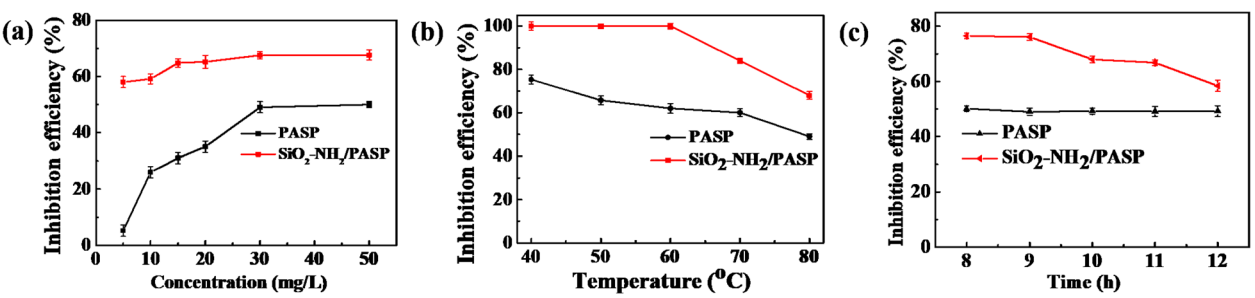

Fig. 4 Inhibition efficiency of PASP and SiO_2–NH_2/PASP against $CaCO_3$ scale. a Different inhibitor concentration, **b** different test temperature, **c** different test time. Error bars indicate the standard deviation.

the solubilization performance of SiO_2-NH_2/PASP on calcium carbonate precipitate is enhanced with the increasing concentration of scale inhibitors. On the other hand, the adsorption capacity of the scale inhibitor and scale crystal is enhanced under increased concentration to reduce the formation of precipitate[32].

The static scale inhibition test temperature and time also have some effects on the inhibition efficiency against the $CaCO_3$ scale. The inhibition performance of SiO_2–NH_2/PASP with 30 mg/L tends to gradually decrease with the increase of the test temperature (Fig. 4b); and its inhibition efficiency maintains at 100% in the test temperature range of 50–70 °C. As the test temperature rises from 70 to 80 °C, the inhibition efficiency of SiO_2–NH_2/PASP decreases from 100 to 68%, but it is still much higher than that of PASP. This indicates that the introduction of SiO_2–NH_2 contributes to improving the scale inhibition performance of PASP at elevated static scale inhibition temperature. With the increase of temperature, the solubility of calcium carbonate decreases, and the formation of calcium carbonate crystals is easier. Meanwhile, temperature also affects the nucleation rate of calcium carbonate, the higher the temperature, the higher the nucleation rate[29].

The effect of static inhibition test time on the inhibition efficiency against the $CaCO_3$ scale is shown in Fig. 4c. The inhibition efficiencies of SiO_2–NH_2/PASP decrease with the increase of time; and it is as much as 76% after 8 h of static scale inhibition test, higher than 50% of PASP under the same test condition. Therefore, it can be inferred that SiO_2–NH_2/PASP has a much stronger chelating ability with Ca^{2+} than PASP.

Characterization of $CaSO_4$ and $CaCO_3$ scales

The crystal morphology exploration tests were repeated three times. The morphology of $CaSO_4$ scales formed under different concentrations of SiO_2–NH_2/PASP and PASP are shown in Fig. S5. The calcium sulfate formed in the presence of SiO_2–NH_2/PASP is of disordered, irregular, and patchy morphology; and that formed after the addition of PASP has a bar-shape morphology as well as increased particle size and length. Figure 5 shows the SEM images of calcium sulfate crystals in the absence and presence of SiO_2–NH_2/PASP scale inhibitor. The $CaSO_4$ crystals formed in the absence of antiscalants have a regular rod-shaped as well as smooth surface and compact crystal structure (Fig. 5a, a′). When 2 mg/L SiO_2–NH_2/PASP is added, $CaSO_4$ crystal with irregular shape and relatively rough surface is formed (Fig. 5d, d′); and $CaSO_4$ macrocrystals in good dispersion state are formed after the addition of 4 mg/L SiO_2–NH_2/PASP (Fig. 5e, e′)[4,33]. As the concentration of PASP increases from 2 to 4 mg/L, strip-like $CaSO_4$ crystal with increased size is formed (Fig. 5b, c, b′, c′). This demonstrates that the introduction of antiscalants, especially SiO_2–NH_2/PASP, leads to significant changes in the morphology as well as average length and diameter of $CaSO_4$ crystals, which could be because the carboxylic group not only can chelate with Ca^{2+} to block the active growth point of $CaSO_4$ crystal but also can dwell on $CaSO_4$ microcrystal surfaces via adsorption to disperse the microcrystal via charge repulsion[10,34]. In other words, the inhibition effect of SiO_2–NH_2/PASP against the $CaSO_4$ scale is dominated by the chelating ability of SiO_2–NH_2/PASP and its adsorption on $CaSO_4$ microcrystal surfaces.

The SEM photographs of $CaCO_3$ crystals formed under different static scale inhibition test conditions are shown in Fig. 6. The $CaCO_3$ crystal obtained without scale inhibitor has a regular shape and smooth surface. With the increase of PASP concentration, the morphology of calcium carbonate becomes disordered and its particle size increases. With 10 mg/L SiO_2–NH_2/PASP, irregular $CaCO_3$ crystal forms, and its sharp edges and acute corners disappear. When the concentration of SiO_2–NH_2/PASP increases to 30 mg/L, the cubic shape of the calcium carbonate scale is destroyed, and its surface is relatively rough; and its shape and size are increased. This could be attributed to two antiscaling mechanisms. On the one hand, the antiscalants can prevent more scale-forming positive ions in the solution from being precipitated through complexation action. On the other hand, the antiscaling chemicals can interact with mineral nuclei to disrupt the crystallization process and keep the crystal particles dispersed in aqueous suspension, thereby inhibiting their sedimentation or adhesion[35,36]. Therefore, it can be inferred that multiple inhibition effects, including lattice distortion, chelation, and dispersion, work together to significantly inhibit the formation of the $CaCO_3$ scale.

The crystal structures of $CaSO_4$ and $CaCO_3$ scales are further analyzed by X-ray diffraction (XRD), and corresponding XRD patterns are shown in Fig. 7. In the absence of the scale inhibitors, the major XRD peaks at $2\theta = 11.53°$, 20.69°, 23.31°, and 29.02° (Fig. 7a) are assigned to gypsum ($CaSO_4{\cdot}2H_2O$). After the addition of SiO_2–NH_2/PASP or PASP, the resultant $CaSO_4$ does not undergo crystal transition, but its crystallization behavior and particle size change to some extent. This further confirms that SiO_2–NH_2/PASP functions to inhibit the formation of $CaSO_4$ scale mainly through chelation and adsorption, which is consistent with relevant SEM results. As to the aqueous solution of $CaCO_3$, calcite and aragonite are the primary crystals formed in the absence of the scale inhibitors (Fig. 7b)[37]. After the addition of SiO_2–NH_2/PASP, the XRD signals of the (104) and (110) planes of calcite disappear, and the strong diffraction peak of vaterite emerges at $2\theta = 29.21°$. Calcite is the most thermodynamically stable, whereas vaterite is the least stable[38,39]. This indicates that SiO_2–NH_2/PASP can inhibit the growth of calcium carbonate crystals and completely block the conversion path from amorphous calcium carbonate to calcite as compared with PASP. In other words, the SiO_2–NH_2/PASP scale

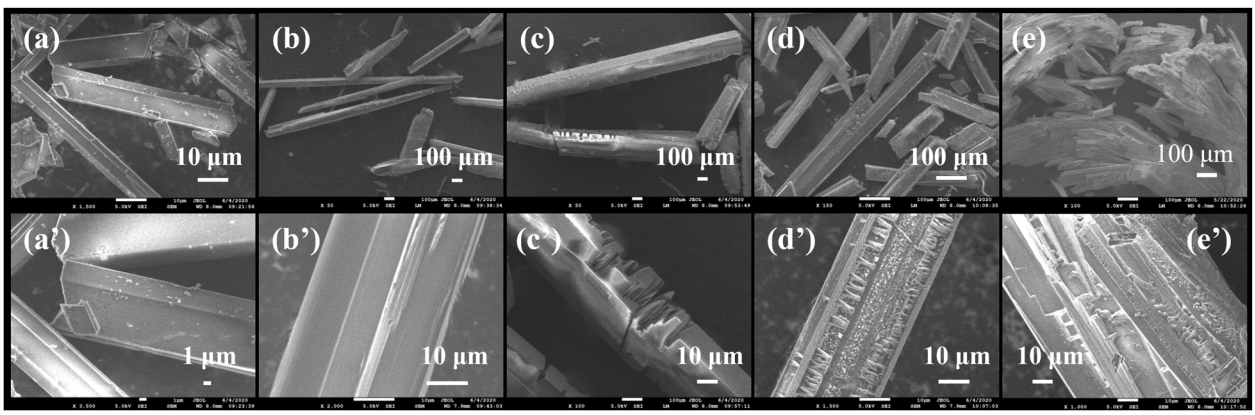

Fig. 5 SEM images of $CaSO_4$ scale at different magnifications. a, **a′** Without antiscalant, **b**, **b′** with 2 mg/L PASP, **c**, **c′** with 4 mg/L PASP, **d**, **d′** with 2 mg/L SiO_2–NH_2/PASP, **e**, **e′** with 4 mg/L SiO_2–NH_2/PASP.

inhibitor functions to inhibit the formation of $CaCO_3$ scale through chelating reaction in association with lattice distortion effect.

Scale inhibition mechanism of SiO_2–NH_2/PASP against $CaSO_4$ and $CaCO_3$

To further explore the adsorption characteristics of SiO_2–NH_2/PASP on scale surface, we conducted X-ray photoelectron spectroscopy (XPS) analyses of the $CaSO_4$ and $CaCO_3$ scales formed under static scale inhibition tests. The high-resolution Ca 2p-XPS spectra of $CaSO_4$ and $CaCO_3$ scales formed without the scale inhibitors and in the presence of PASP and SiO_2–NH_2/PASP are given in Figs. 8 and 9. In the absence of the scale inhibitors, the $CaSO_4$ scale shows the distinctive peaks of Ca $2p_{1/2}$ and Ca $2p_{3/2}$ at 351.42 and 347.84 eV, respectively (Fig. 8). After the addition of 4 mg/L PASP, the Ca $2p_{1/2}$ and Ca $2p_{3/2}$ peaks shift to 351.53 and 347.93 eV, which corresponds to a change in the chemical surroundings of Ca^{2+} ion upon the introduction of PASP. The Ca $2p_{1/2}$ and Ca $2p_{3/2}$ peaks further shift to 351.58 and 347.99 eV after the addition of 4 mg/L SiO_2–NH_2/PASP, which gives further evidence to the uptake of scale inhibitors on the surface of calcium sulfate scales. Similarly, the introduction of PASP and SiO_2–NH_2/PASP leads to shifting in the Ca 2p peaks of the $CaCO_3$ scale by 0.17 and 0.42 eV, respectively (Fig. 9). These findings imply that the SiO_2–NH_2/PASP scale inhibitor can be adsorbed on the surface of $CaSO_4$ and $CaCO_3$ scales to affect the growth, morphology, and size of scales, thereby effectively retarding their formation in aqueous solutions.

The inhibition mechanism of SiO_2–NH_2/PASP against $CaSO_4$ and $CaCO_3$ scales is shown in Fig. 10. In the absence of the scale inhibitors, calcium sulfate and calcium carbonate form stable scales on the pipe surface, as shown in Fig. 10a, b. When SiO_2–NH_2/PASP is dissolved in water, the negatively charged carboxylic group of SiO_2–NH_2/PASP coordinates with positively charged Ca^{2+} ions to prevent them from forming calcium carbonate and sulfate. Meanwhile, SiO_2–NH_2/PASP can be

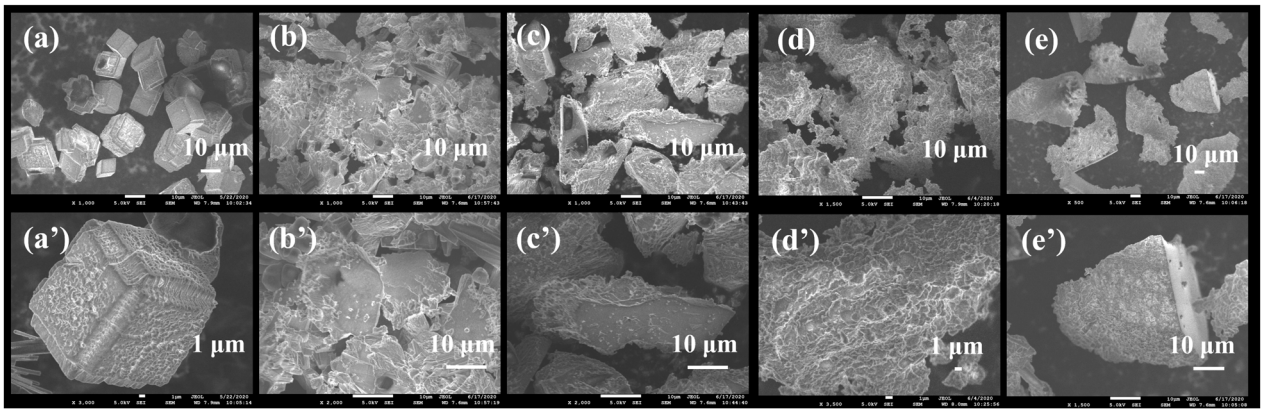

Fig. 6 SEM images of $CaCO_3$ scale at different magnifications. a, **a'** Without antiscalant, **b**, **b'** with 10 mg/L PASP, **c**, **c'** with 30 mg/L PASP, **d**, **d'** with 10 mg/L SiO_2-NH_2/PASP, **e**, **e'** with 30 mg/L SiO_2–NH_2/PASP.

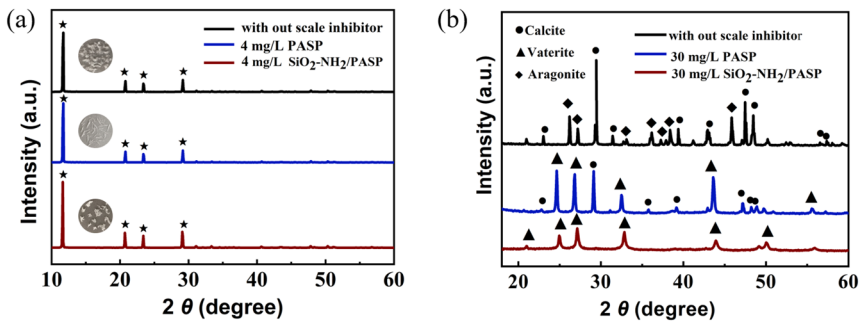

Fig. 7 XRD patterns of an aqueous solution of scale. a $CaSO_4$ scale, **b** $CaCO_3$ scale.

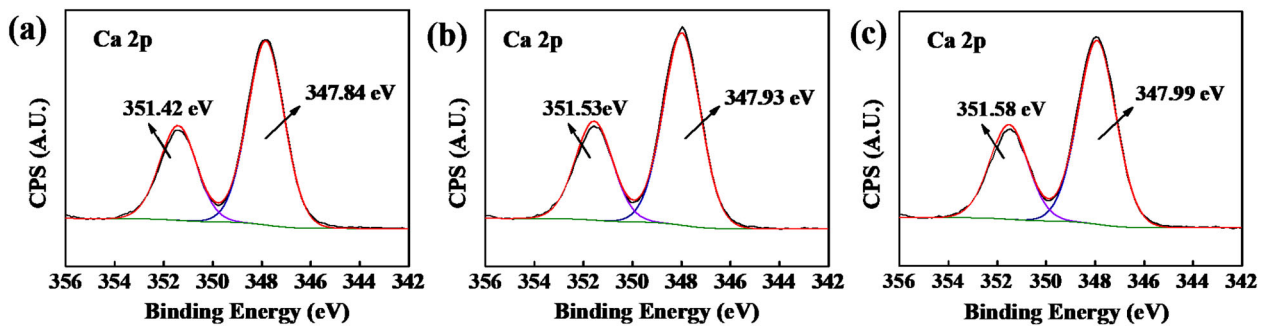

Fig. 8 Ca 2p XPS spectra of $CaSO_4$ scales. a Without scale inhibitor, **b** with 4 mg/L PASP, **c** with 4 mg/L SiO_2–NH_2/PASP.

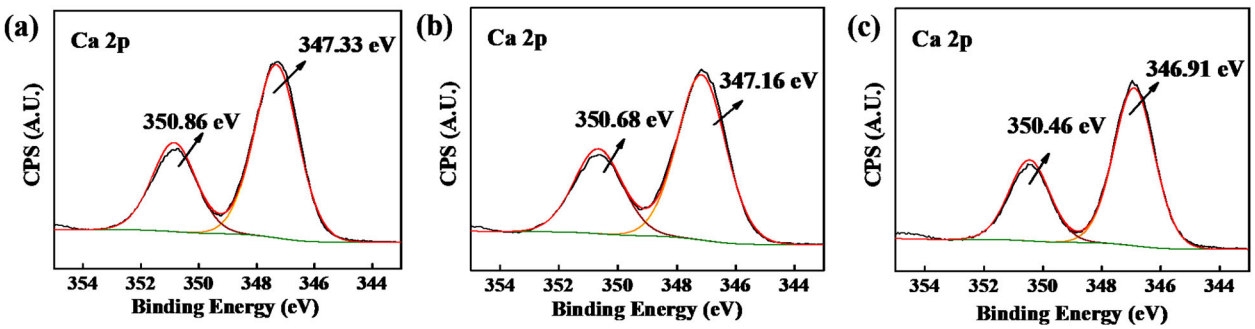

Fig. 9 Ca2p XPS spectra of $CaCO_3$ scales. a Without scale inhibitor, **b** with 30 mg/L PASP, **c** with 30 mg/L SiO_2–NH_2/PASP.

adsorbed on the surface of newly generated scale crystal to increase the inter-particle repulsive force and prevent intercrystalline bonding, thereby accommodating good dispersion of the scales and retarding their deposition on the inner walls of the pipes (Fig. 10c, d). As a result, SiO_2–NH_2/PASP can effectively inhibit the formation of $CaSO_4$ and $CaCO_3$ scales in aqueous solutions.

In summary, SiO_2–NH_2/PASP, an organic-inorganic hybrid as a potential green scale inhibitor for industrial circulating water, is synthesized via a facile liquid-phase polymerization route. Static scale inhibition tests demonstrate that SiO_2–NH_2/PASP exhibits much better inhibition performance against $CaSO_4$ and $CaCO_3$ scales than PASP, and has good environmental adaptability. This is because, as evidenced by SEM, XRD, and XPS analyses, the carboxylic group of SiO_2–NH_2/PASP can chelate with Ca^{2+} to block the active growth points of the inorganic scales while its adsorption on scale crystal surface also contributes to retarding the formation of the scales. Furthermore, SiO_2–NH_2/PASP can completely change the conversion path from amorphous calcium carbonate to calcite, which could also account for its desired inhibition ability against the $CaCO_3$ scale. The as-prepared SiO_2–NH_2/PASP scale inhibitor with good environmental acceptance could be promising in preventing the formation of $CaSO_4$ and $CaCO_3$ scales on the inner walls of the pipes for industrial circulating water.

METHODS

Materials

Reactive nanosilica (SiO_2–NH_2) surface modified with amino (adsorption aperture: 19.2 nm) was provided by Henan Wangwu Nanotechnology Company Limited (Jiyuan, China). Industrial grade polysuccinimide (PSI, $M_w = 7000$) was purchased from Wuhan Yuancheng Gongyi Technology Company Limited (Wuhan, China). Anhydrous calcium chloride, disodium edetate, anhydrous sodium sulfate, borax, and potassium hydroxide were purchased from Tianjin Komi Chemical Reagent Company Limited (Tianjin, China). Anhydrous sodium hydrogencarbonate was commercially obtained from Tianjin Deen Chemical Reagent Company Limited (Tianjin, China). Anhydrous ethanol was bought from Anhui Ante Food Company Limited (Suzhou, China). Deionized water (DI) was used as the solvent and for rinsing as well.

Preparation of SiO_2–NH_2/PASP

A certain amount of SiO_2–NH_2 was dispersed in the mixed solution of ethanol and DI. The as-obtained dispersion (0.013 g) was placed into a round bottom flask, followed by the addition of 0.984 g of PSI under stirring at 60 °C for 1 h. The resultant mixed dispersion was allowed to react for 24 h thereat while its pH was adjusted to be 8–9. Upon completion of the reaction, the product was precipitated with absolute ethanol for 12 h and dried at 60 °C for 24 h to afford SiO_2–NH_2/PASP solid product. PASP was prepared in the same manner while no SiO_2–NH_2 was used[19].

Characterization of SiO_2-NH_2/PASP

The morphology of SiO_2–NH_2 nanohybrid was observed with a transmission electron microscope (TEM; JEM-2010, JEOL, Japan). The structure of SiO_2–NH_2/PASP was characterized by Fourier transform infrared spectroscopy (VERTEX 70 FTIR spectrometer, Bruker Optics, Germany), 1H nuclear magnetic resonance spectroscopy (^{1}H NMR; AVANCE 400 MHz NMR spectrometer, Bruker Optics, Germany), and scanning electron microscopy inconnection with energy dispersive spectrometry (SEM-EDS; JSM-7610F, Hitachi, Japan).

The carboxyl content of PASP and SiO_2–NH_2/PASP was determined by conductance titration. First, excess HCl solution was added to acidize PASP and SiO_2–NH_2/PASP, then titrated with NaOH standard solution, and the volume and conductivity values of the consumed NaOH standard solution were recorded[40]. The conductivity curve is shown in Fig. S6. The carboxyl group content (W) can be calculated by Eq. (2)[40]

$$W = \frac{M \times (V_2 - V_1) \times 45}{1000m} \times 100\ \% \quad (2)$$

M is the concentration of the NaOH solution, mol/L; V_1 is the volume of the NaOH standard solution consumed by excess hydrochloric acid, mL; V_2 is the volume of the NaOH standard solution consumed by excess hydrochloric acid and the carboxyl group contained in the polymer, mL; V_2–V_1 is the volume of the standard solution of NaOH consumed by the carboxyl group in the polymer, mL; W is the mass of the sample, g[40].

Static scale inhibition tests

The antiscalant performance of SiO_2–NH_2/PASP against calcium sulfate was tested by the static scale inhibition method. Briefly, proper amounts of $CaCl_2$ (6800 mg/L Ca^{2+}) and Na_2SO_4 (7100 mg/L of SO_4^{2-}) were mixed at 70 °C for 6 h; and the filtrate was titrated with ethylene diamine tetraacetic acid (EDTA) standard solution to determine the concentration of calcium ion. The scale inhibition efficiency (E, %) against $CaSO_4$ is calculated as

$$E = \frac{X_2 - X_1}{X_0 - X_1} \times 100\ \% \quad (3)$$

where X_0 (mg/L) is the initial concentration of Ca^{2+} in the water samples before heating, X_2 and X_1 (mg/mL) are the concentration of Ca^{2+} after reaction in the presence and absence of scale inhibitor, respectively. The static inhibition tests were repeated three times, and the average of the repeat tests was cited to minimize data scattering.

An aqueous solution containing 240 mg/L Ca^{2+} and 732 mg/L HCO_3^- was prepared and heated with a water bath at 80 °C for 10 h. At the end of heating, the solution was cooled to room temperature; and the Ca^{2+} concentration in the supernatant was determined by EDTA titration. The scale inhibition efficiency (η, %) against $CaCO_3$ is calculated as

$$\eta = \frac{C_2 - C_1}{C_0 - C_1} \times 100\ \% \quad (4)$$

where C_0 (mg/mL) is the concentration of Ca^{2+} in the solution before the static inhibition test, C_1 and C_2 (mg/mL) are the concentration of Ca^{2+} in the absence and presence of scale inhibtor, respectively. All the static inhibition tests were conducted in triplicate to ensure reproducibility.

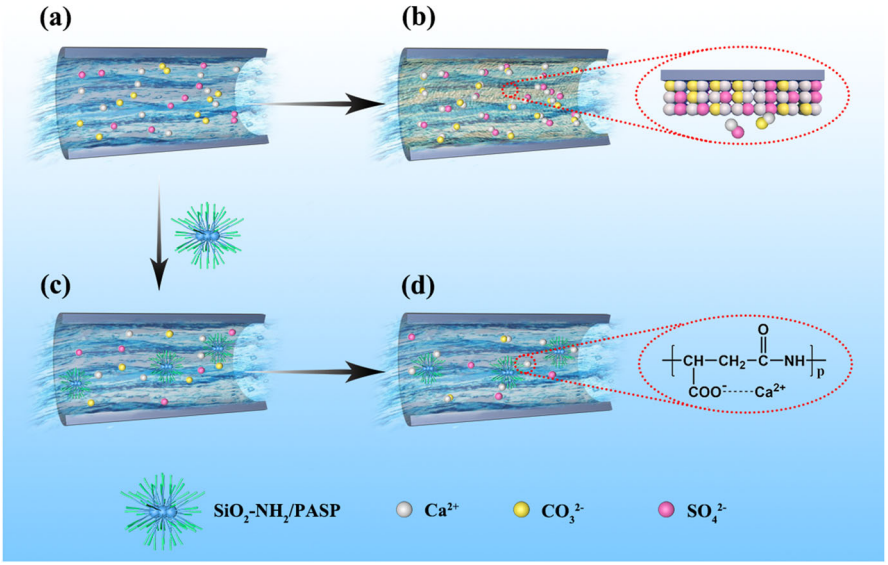

Fig. 10 Schematic illustration of inhibition mechanism of SiO_2–NH_2/PASP against $CaSO_4$ and $CaCO_3$ scales. a The inside of the pipe without heating and adding SiO_2–NH_2/PASP, **b** the inside of the pipe after heating, **c** the inside of the pipe after adding SiO_2–NH_2/PASP, **d** the inside of the pipe after heating and adding SiO_2–NH_2/PASP.

Surface analysis of scale crystal

The surface morphology of the as-formed scale crystal was observed with a scanning electron microscope (JSM-7610F, JOEL, Japan); and its crystal configuration was identified by XRD (D8 Advance, Bruker Optics, Germany). Moreover, the interaction between the scale inhibitor and scale crystals was investigated by XPS (ESCALAB 250Xi, Thermo, USA; monochromated Al K_α X-ray source, $hv = 1486.6$ eV).

DATA AVAILABILITY

All data needed to evaluate the conclusion in this paper are presented in the paper.

Received: 19 March 2021; Accepted: 11 August 2021;
Published online: 23 September 2021

REFERENCES

1. Rahman, F. Calcium sulfate precipitation studies with scale inhibitors for reverse osmosis desalination. *Desalination* **319**, 79–84 (2013).
2. Ali, S. A., Kazi, I. W. & Rahman, F. Synthesis and evaluation of phosphate-free antiscalants to control $CaSO_4{\cdot}2H_2O$ scale formation in reverse osmosis desalination plants. *Desalination* **357**, 36–44 (2015).
3. Al-Roomi, Y. M. & Hussain, K. F. Potential kinetic model for scaling and scale inhibition mechanism. *Desalination* **393**, 186–195 (2016).
4. Zhang, Z.-j et al. Fluorescent-tagged hyper-branched polyester for inhibition of $CaSO_4$ scale and the scale inhibition mechanism. *Mater. Today Commun.* **25**, 101359 (2020).
5. Feoktistova, N. et al. Controlling the vaterite $CaCO_3$ crystal pores. design of tailor-made polymer based microcapsules by hard templating. *Langmuir* **32**, 4229–4238 (2016).
6. Suharso, R., Endaryanto, T. & Buhani. Modification of gambier extracs as green inhibitor of calcium carbonate ($CaCO_3$) scale formation. *J. Water Process Eng.* **18**, 1–6 (2017).
7. Wang, H., Gao, M., Guo, Y., Yang, Y. & Hu, R. A natural extract of tobacco rob as scale and corrosion inhibitor in artificial seawater. *Desalination* **398**, 198–207 (2016).
8. Wang, Y. et al. Synthesis and characterization of PBTCA-modified hyperbranched polyether corrosion and scale inhibitors. *J. Appl. Polym. Sci.* **136**, 48041 (2019).
9. Chaussemier, M. et al. State of art of natural inhibitors of calcium carbonate scaling. a review article. *Desalination* **356**, 47–55 (2015).
10. Yu, W., Wang, Y., Li, A. & Yang, H. Evaluation of the structural morphology of starch-graft-poly(acrylic acid) on its scale-inhibition efficiency. *Water Res.* **141**, 86–95 (2018).
11. He, C. et al. Inhibition effect of environment-friendly inhibitors on the corrosion of carbon steel in recirculating cooling water. *Ind. Eng. Chem. Res.* **54**, 1971–1981 (2015).
12. Zhang, Y., Yin, H., Zhang, Q., Li, Y. & Yao, P. Synthesis and characterization of novel polyaspartic acid/urea graft copolymer with acylamino group and its scale inhibition performance. *Desalination* **395**, 92–98 (2016).
13. Zhang, Y. et al. A novel polyaspartic acid derivative with multifunctional groups for scale inhibition application. *Environ. Technol.* **39**, 843–850 (2018).
14. Migahed, M. A., Rashwan, S. M., Kamel, M. M. & Habib, R. E. Synthesis, characterization of polyaspartic acid-glycine adduct and evaluation of their performance as scale and corrosion inhibitor in desalination water plants. *J. Mol. Liq.* **224**, 849–858 (2016).
15. Chen, Y., Xing, W., Wang, L. & Chen, L. Experimental and electrochemical research of an efficient corrosion and scale inhibitor. *Materials* **12**, 1821 (2019).
16. Yuan, X., Dong, S., Zheng, Q., Yang, W. & Huang, T. Novel and efficient curcumin based fluorescent polymer for scale and corrosion inhibition. *Chem. Eng. J.* **389**, 124296 (2020).
17. Chen, Y., Chen, X. & Liang, Y. Synthesis of polyaspartic acid/graphene oxide grafted copolymer and evaluation of scale inhibition and dispersion performance. *Diam. Relat. Mater.* **108**, 107949 (2020).
18. Chen, J. et al. A green multifunctional antiscaling inhibitor for crystallization control of Ca-scale crystals. *Chem. Eng. Technol.* **42**, 444–453 (2019).
19. Shi, S., Wu, Y., Wang, Y., Yu, J. & Xu, Y. Synthesis and characterization of a biodegradable polyaspartic acid/2-amino-2-methyl-1-propanol graft copolymer and evaluation of its scale and corrosion inhibition performance. *RSC Adv.* **7**, 36714–36721 (2017).
20. Hasson, D., Shemer, H. & Sher, A. State of the art of friendly "green" scale control inhibitors: a review article. *Ind. Eng. Chem. Res.* **50**, 7601–7607 (2011).
21. Xie, L. et al. Preparation and properties of long chain branched high-density polyethylene based on nano-SiO_2 grafted glycidyl methacrylate. *RSC Adv.* **9**, 1123–1133 (2019).
22. Qin, W., Hou, J. & Bonnell, D. A. Effect of interface atomic structure on the electronic properties of nano-sized metal-oxide interfaces. *Nano Lett.* **15**, 211–217 (2015).
23. Fotticchia, I. et al. Thermodynamic signature of secondary nano-emulsion formation by isothermal titration calorimetry. *Langmuir* **30**, 14427–14433 (2014).
24. Cao, T. T., Yabu, H. & Huh, D. S. Hierarchical nano/micro moth eyelike polymer film using solid/liquid interfacial reaction at room temperature. *Langmuir* **36**, 9064–9073 (2020).
25. Chai, C. et al. Cysteamine modified polyaspartic acid as a new class of green corrosion inhibitor for mild steel in sulfuric acid medium: Synthesis, electrochemical, surface study and theoretical calculation. *Prog. Org. Coat.* **129**, 159–170 (2019).

26. Cheng, Y. et al. Water-dispersible reactive nanosilica and poly(2-acrylamido-2-methyl-1-propanesulfonic acid sodium) nanohybrid as potential oil displacement agent for enhanced oil recovery. *Energ. Fuel* **31**, 6345–6351 (2017).
27. Zhang, S. et al. Scale inhibition performance and mechanism of sulfamic/amino acids modified polyaspartic acid against calcium sulfate. *Desalination* **419**, 152–159 (2017).
28. Boerlage, S. et al. The scaling potential of barium sulphate in reverse osmosis systems. *J. Membr. Sci.* **197**, 251–268 (2002).
29. Yu, W., Song, D., Chen, W. & Yang, H. Antiscalants in RO membrane scaling control. *Water Res.* **183**, 115985 (2020).
30. Jawor, A. & Hoek, E. Effects of feed water temperature on inorganic fouling of brackish water RO membranes. *Desalination* **235**, 44–57 (2009).
31. El-Shall, H., Rashad, M. M. & Abdel-Aal, E. A. Effect of cetyl pyridinium chloride additive on crystallization of gypsum in phosphoric and sulfuric acids medium. *Cryst. Res. Technol.* **40**, 860–866 (2005).
32. Ray, J. R., Wong, W. & Jun, Y. S. Antiscaling efficacy of $CaCO_3$ and $CaSO_4$ on polyethylene glycol (PEG)-modified reverse osmosis membranes in the presence of humic acid: interplay of membrane surface properties and water chemistry. *Phys. Chem. Chem. Phys.* **19**, 5647–5657 (2017).
33. Liu, G., Xue, M. & Yang, H. Polyether copolymer as an environmentally friendly scale and corrosion inhibitor in seawater. *Desalination* **419**, 133–140 (2017).
34. Hong, Y., Yufit, D. S., Letzelter, N. & Steed, J. W. Calcium cyclic carboxylates as structural models for calcium carbonate scale inhibitors. *CrystEngComm* **22**, 2585–2592 (2020).
35. Deng, H., Wang, X.-M., Du, C., Shen, X.-C. & Cui, F.-Z. Combined effect of ion concentration and functional groups on surface chemistry modulated $CaCO_3$ crystallization. *CrystEngComm* **14**, 6647–6653 (2012).
36. Sheikhi, A., Kakkar, A. & van de Ven, T. G. M. Biomimetic scale-resistant polymer nanocomposites: towards universal additive-free scale inhibition. *J. Mater. Chem. A* **6**, 10189–10195 (2018).
37. Zhu, Y., Li, H., Zhu, M., Wang, H. & Li, Z. Dynamic and active antiscaling via scale inhibitor pre-stored superhydrophobic coating. *Chem. Eng. J.* **403**, 126467 (2021).
38. Liu, G. et al. Maleic anhydride–allylpolyethoxy carboxylate copolymer as an effective and environmentally benign inhibitor for calcium carbonate in industrial cooling systems. *RSC Adv.* **7**, 24723–24729 (2017).
39. Zuo, Z. et al. Effect of scale inhibitors on the structure and morphology of $CaCO_3$ crystal electrochemically deposited on TA1 alloy. *J. Colloid Interface Sci.* **562**, 558–566 (2020).
40. Cai, S. *Characterization of Physical and Chemical Properties of Polyepoxysuecinic Acid [D].* (Beijing University of Chemical Technology, Beijing, 2004).

ACKNOWLEDGEMENTS

This work is funded by the Ministry of Science and Technology of China (in the name of State Key Research and Development Plan; grant No. SQ2020YFF0402903). We would like to express our gratitude to Professor Yu Laigui from the National & Local Joint Engineering Research Center for Applied Technology of Hybrid Nanomaterials for their valuable comments and his careful revision of the paper.

AUTHOR CONTRIBUTIONS

Y.C.: Conceptualization, investigation, writing—original draft. X.G.: Conceptualization, investigation, writing—original draft. X.Z.: Formal analysis and investigation. Y.W.: Investigation, writing—review and editing. Z.C.: Writing—review and editing. Y.C.: Conceptualization, supervision, writing—review and editing. Y.X.: Resources, supervision, and funding acquisition.

COMPETING INTERESTS

The authors declare no competing interests.

ADDITIONAL INFORMATION

Supplementary information The online version contains supplementary material available at https://doi.org/10.1038/s41545-021-00137-y.

Correspondence and requests for materials should be addressed to Yonghong Cai or Ying Xu.

Reprints and permission information is available at http://www.nature.com/reprints

Publisher's note Springer Nature remains neutral with regard to jurisdictional claims in published maps and institutional affiliations.

Open Access This article is licensed under a Creative Commons Attribution 4.0 International License, which permits use, sharing, adaptation, distribution and reproduction in any medium or format, as long as you give appropriate credit to the original author(s) and the source, provide a link to the Creative Commons license, and indicate if changes were made. The images or other third party material in this article are included in the article's Creative Commons license, unless indicated otherwise in a credit line to the material. If material is not included in the article's Creative Commons license and your intended use is not permitted by statutory regulation or exceeds the permitted use, you will need to obtain permission directly from the copyright holder. To view a copy of this license, visit http://creativecommons.org/licenses/by/4.0/.

© The Author(s) 2021